A Numerical and Experimental Study of Reaction Front Propagation in Condensed Phase Systems

J. Puszynski, S. Kumar, P. Dimitriou, and V. Hlavacek

Department of Chemical Engineering State University of New York at Buffalo, Buffalo, New York, USA

Z. Naturforsch. **43a**, 1017–1025 (1988); received September 1, 1988

Certain noncatalytic exothermic chemical reactions of the type solid-solid characterized by high values of activation energy and heat of reaction represent an example of strongly nonlinear chemically reacting systems. In these systems different types of propagating waves can be observed such as constant pattern, planar pulsating, and rotating waves. Numerical simulations in two and three spatial dimensions predict, qualitatively, the same behavior as experimentally observed. For geometrically large systems multihead spinning or erratic waves occur, which bifurcate from a planar pulsating front. In nonadiabatic systems the spinning wave is more resistant to extinction than the one-dimensional planar pulsating front.

List of Symbols

C	concentration, kg m^{-3}
C_p	heat capacity, J kg^{-1} K^{-1}
d	diameter, m
E	activation energy, J mol^{-1}
K_0	rate constant
K_H	heat transfer coefficient, J m^{-2} s^{-1} K^{-1}
R_g	universal gas constant, J mol^{-1} K^{-1}
R	radius of sample, m
r	radial coordinate, m
rate	reaction rate, mol m^{-3} s^{-1}
t	time, s
$t_* = \frac{(\varrho C_p) R_g T_*^2 \exp(E/R_g T_*)}{E k_0 (-\Delta H) C_{S0}}$	reference time, s
T	temperature, K
$u = z\sqrt{\varrho C_p/\lambda t_*}$	dimensionless axial coordinate
z	axial coordinate, *m*.

Greek Symbols

$\alpha = 4 K_H/d$	dimensionless heat transfer coefficient
$\beta = R_g T_*/E$	dimensionless activation energy
$\gamma = \frac{\varrho C_p R_g T_*^2}{C_0 E(-\Delta H)}$	dimensionless heat of reaction
ΔH	heat of reaction, J kg^{-1}
$\eta = 1 - C_S/C_{S0}$	conversion
$\theta = \frac{E}{R_g T_*^2}(T - T_*)$	dimensionless temperature
λ	heat conductivity, J m^{-1} s^{-1} K^{-1}
$\nu = \lambda t_*/\varrho C_p \pi^2 d^2$	dimensionless circumference
$\xi = r/R$	dimensionless radial coordinate
ϱ	density, kg m^{-3}
τ	dimensionless time
ϕ	angular coordinate
$\Phi = \phi/2\pi$	dimensionless angular coordinate

Subscripts

i	ignition
o	initial
s	solid
$*$	reference

Introduction

There exists an important class of condensed phase reactions, characterized by large heat generation and large values of activation energy, that represents strongly nonlinear chemically reacting systems. The most important examples are: reduction of certain metallic oxides by powdered aluminum, reduction of boric oxide by magnesium to elemental boron, and synthesis of transition metal compounds such as carbides, borides and silicides [1–4]. These reactions, when initiated locally by an external energy source, with short term service, may propagate throughout the sample at a certain rate and occur in a narrow zone which separates the fresh reactants from the reaction products. This type of process is termed self-propagating high temperature synthesis (SHS). The advantage of this combustion technology is effective utilization of thermal energy released during the reaction.

The linear stability analysis of propagating reaction fronts in condensed phases was based on the assumption of an infinitesimal thin reaction front to predict the regions of spatial instabilities [5–11]. However, for finite values of activation energy, this assumption may

Reprint requests to Prof. V. Hlavacek, Department of Chemical Engineering, University at Buffalo, Clifford C. Furnas Hall, Buffalo, New York 14260, USA.

0932-0784 / 88 / 1200-1017 $ 01.30/0. – Please order a reprint rather than making your own copy.

lead to deviations from the results obtained by numerical solution of complete heat and mass balance equations*. So far little attention has been payed to predict the onset as well as full development of propagating waves in two [13] and three spatial dimensions.

The objective of this work is to present 2D and 3D numerical results as well as experimental observations on wave propagation in condensed phase systems.

Model Formulation and Numerical Solution

The mathematical model of gasless combustion is based on the following physical assumptions:

1. A heterogeneous mixture of solid reactants behaves as an isotropic homogeneous system.
2. The reaction rate expression is taken as first-order with respect to the limiting reactant and has Arrhenius form of temperature dependence.
3. Heat conduction in the solid phase is described by Fourier's law.
4. All physical properties (density, heat capacity, effective thermal conductivity) are constant.
5. The reaction is not accompanied by melting effects.
6. Heat loss from the system is described by the Newton's law of cooling.

Heat and mass balance are described by the following equations:

$$\langle \varrho\, c_p \rangle \frac{\mathrm{d}T}{\mathrm{d}t} = \lambda \left(\frac{\partial^2 T}{\partial z^2} + \frac{1}{r}\frac{\partial}{\partial r}\left(r \frac{\partial T}{\partial r} \right) + \frac{1}{r^2}\frac{\partial^2 T}{\partial \phi^2} \right) + k(-\Delta H) C_S, \tag{1}$$

$$\partial C_S / \partial t = -k C_S. \tag{2}$$

For the meaning of the symbols cf. the list at the end of the paper.

The initial conditions are:

$$t = 0; \quad 0 \leqq z < \infty, \quad 0 \leqq \phi \leqq 2\pi, \quad 0 \leqq r \leqq R, \quad T = T_0,\ C_S = C_{S0}. \tag{3}$$

The boundary conditions are:

$$t > 0; \quad z = 0, \quad 0 \leqq r \leqq R, \quad 0 \leqq \phi \leqq 2\pi: \quad T = T_i,$$
$$z \to \infty, \quad 0 \leqq r \leqq R, \quad 0 \leqq \phi \leqq 2\pi: \quad T = T_0, \tag{4}$$
$$0 < z < \infty, \quad 0 \leqq r \leqq R, \quad 0 \leqq \phi \leqq 2\pi: \quad T(t, z, r, \phi) = T(t, z, r, \phi + 2\pi),$$
$$0 < z < \infty, \quad r = R, \quad 0 \leqq \phi \leqq 2\pi: \quad \lambda \frac{\partial T}{\partial r} = h(T - T_0).$$

For the purpose of the numerical simulation it is more convenient to rewrite (1) to (4) in dimensionless form:

$$\frac{\partial \theta}{\partial \tau} = \frac{\partial^2 \theta}{\partial u^2} + v\left(4\pi^2 \frac{1}{\xi}\frac{\partial}{\partial \xi}\left(\xi \frac{\partial \theta}{\partial \xi} \right) + \frac{1}{\xi^2}\frac{\partial^2 \theta}{\partial \Phi^2} \right) + (1 - \eta) \exp\left(\frac{\theta}{1 + \beta\theta} \right), \tag{5}$$

$$\frac{\partial \eta}{\partial \tau} = \gamma (1 - \eta) \exp\left(\frac{\theta}{1 + \beta\theta} \right). \tag{6}$$

The initial and the boundary conditions are:

$$\tau = 0; \quad 0 \leqq u < \infty, \quad 0 \leqq \xi \leqq 1, \quad 0 \leqq \Phi \leqq 1: \quad \theta = \theta_0, \quad \eta = 0. \tag{7}$$

$$\tau > 0; \quad u = 0, \quad 0 \leqq \xi \leqq 1, \quad 0 \leqq \Phi \leqq 1: \quad \theta = \theta_i,$$
$$u \to \infty, \quad 0 \leqq \xi \leqq 1, \quad 0 \leqq \Phi \leqq 1: \quad \theta = \theta_0, \tag{8}$$
$$0 < u < \infty, \quad 0 \leqq \xi \leqq 1, \quad 0 \leqq \Phi \leqq 1: \quad \theta(\tau, u, \xi, \Phi) = \theta(\tau, u, \xi, \Phi + 1),$$
$$0 < u < \infty, \quad \xi = 1, \quad 0 \leqq \Phi \leqq 1: \quad \frac{\partial \theta}{\partial \xi} = \alpha(\theta - \theta_0).$$

The dimensionless temperature (θ), conversion (η), activation energy (β), heat of reaction (γ), time (τ), and space coordinates (u, ξ, Φ) are defined in the list of symbols.

Numerical solution of the governing equations (5) and (6) under the conditions (7) and (8) represents a difficult problem. The "boundary layers" on concentration and temperature spatial profiles require a good resolution, otherwise artificial oscillations may occur in the numerical solution.

The integration in time is first order implicit with an automatic time step adjustment. The time step is adjusted automatically depending upon the rate of reaction [14]. The space derivatives are approximated by centered finite differences on an adaptive moving mesh. The idea behind moving meshes is the enhancement of the resolution by clustering a fixed number of points at the appropriate places, i.e., in regions of high gradients or large curvature [14, 15].

The use of adaptive meshes makes the simulations in two and three spatial dimensions computationally

* For the one-dimensional case see [12].

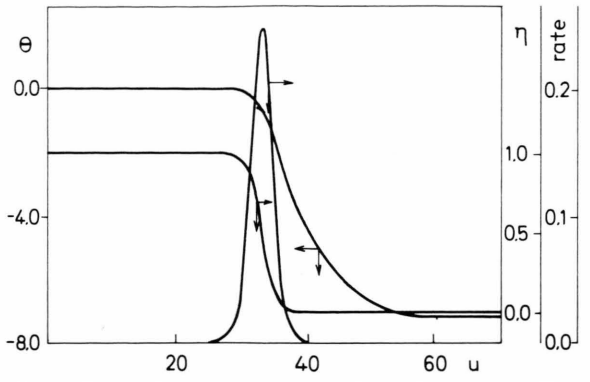

Fig. 1. Conversion, temperature and reaction rate profiles-planar, stable combustion regime ($\beta = 0.0645$, $\gamma = 0.14$, $\Theta_0 = -7.14$, $\Theta_i = 0.0$, $\alpha = 0.0$).

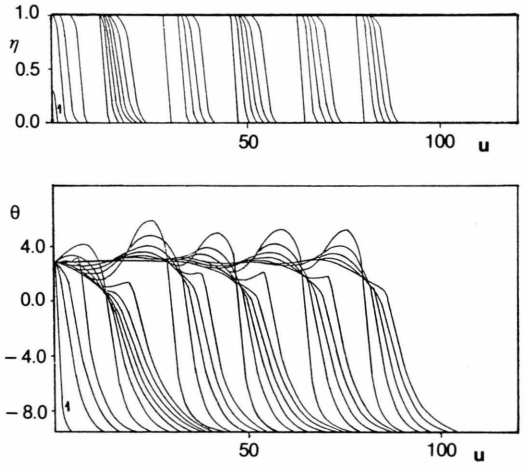

Fig. 2. Time-space conversion and temperature profiles ($\beta = 0.03$, $\gamma = 0.08$, $\Theta_0 = -9.5$, $\Theta_i = 3.0$, $\alpha = 0.0001$, $\Delta\tau = 10$). First profile at time $\tau = 10$ and succeeding 31 profiles at constant time increments of $\Delta\tau = 10$.

efficient since the memory space as well as the number of operations required are much lower than for equidistant meshes with the same spatial resolution.

Numerical Observation

The asymptotic analysis of the exothermic reaction front propagation assumes that the reaction zone is infinitesimally thin. However, this assumption can lead to considerable deviations from the exact results. For instance, the value of the Hopf bifurcation point calculated analytically may differ from the exact value, determined by numerical simulation by as much as 20% [12]. A typical distribution of temperature, conversion and reaction rate for a planar nonpulsating front is given in Figure 1. In a pulsating regime the velocity of the propagating front and, therefore, temperature and conversion oscillate with respect to time. Time-space concentration and temperature profiles in such a regime are shown in Figure 2.

Two Dimensional Simulations

Depending on the governing parameters, the reaction front can propagate either as a planar constant pattern profile or a planar pulsating wave [12]. The model equations (1–4) were solved numerically for parameter values that gave a planar pulsating solution.

Small sinusoidal as well as step perturbations in temperature and/or concentration were imposed in order to locate the nonplanar families of solution. It should be mentioned that the reaction front remained planar as long as no perturbation was imposed.

For better presentation we have plotted our results in the form of color patterns. Each time frame represents the cylindrical section of a hollow cylinder opened to form a two dimensional rectangular sheet. In Fig. 3 a planar pulsating temperature wave is shown. It can be seen clearly in the frames for $\tau > 480$ that a small perturbation in temperature introduced at $\tau = 480$, decays. However, a strong step perturbation in temperature when introduced during the heat-up period of the process results in breaking of symmetry. For these conditions and type of perturbation a nonplanar wave was generated as shown in Figure 4. The highest reaction rate is at the inflection point on the axial concentration profile. Behind this inflection point the concentration of the fuel is higher, however the reaction rate is lower. As a result, islands of fuel remain in the completely reacted material (see frame 75). The complete conversion of the solid reactants within these islands is reached well behind the reaction front (after burning phenomena). In the region of high reaction rate (white region in frame 70) the fuel is consumed and a cooling-down process occurs. Since there are large axial and angular temperature gradients, the reaction is initiated where a relatively cool fuel with low degree of conversion is available. Here the reaction process is ignited and a new finger created.

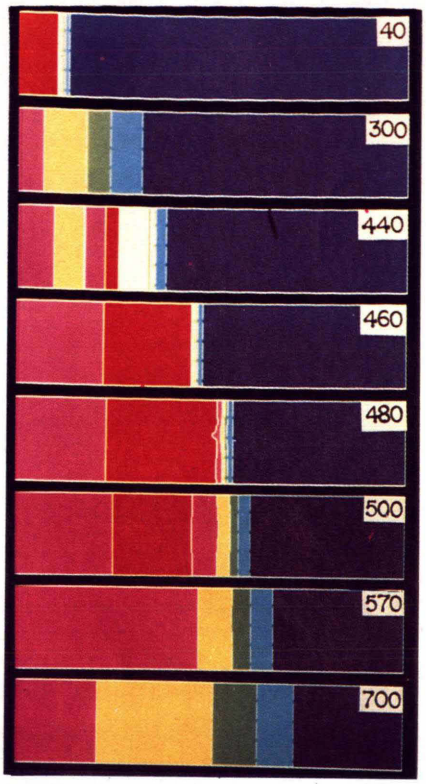

Fig. 3. Planar pulsating front (2D case), ($\beta = 0.03$, $\gamma = 0.08$, $\Theta_0 = -9.5$, $\Theta_i = 3.0$, $\vartheta = 0.001$, $\alpha = 0.001$). Numbers are values of τ. Colors represent values of Θ. Dimensionless temperature range: blue (-9.5; -7.0); cyan (-7.0; -4.5); green (-4.5; -2.0); yellow (-2.0; 0.5); magenta (0.5; 3.0); red (3.0; 5.5); white (5.5; 8.0).

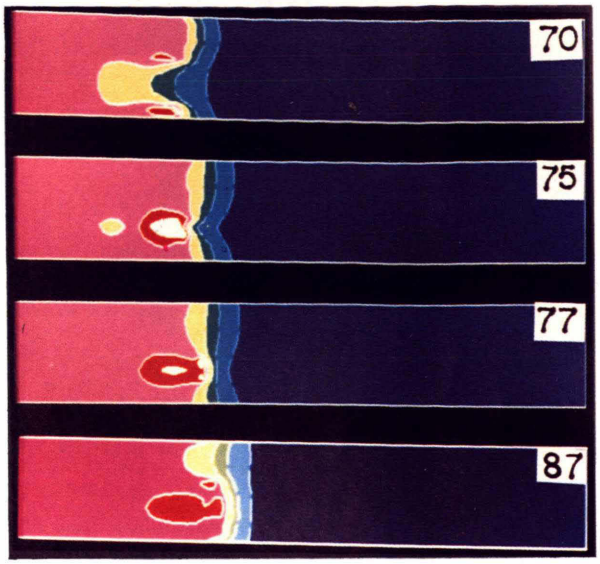

Fig. 4. Nonplanar wave (2D case), ($\beta = 0.03$, $\gamma = 0.08$, $\Theta_0 = -9.5$, $\Theta_i = 3.0$, $\nu = 0.001$, $\alpha = 0.001$).

In Fig. 5 a rotating wave is displayed. An asymmetrical perturbation in concentration and temperature was imposed during the heating up period and a helical movement resulted. Here the hot spot (see the white region) follows on the cylindrical surface a screw-like path. We can notice the travelling wave along the interface (cf. the yellow region). The rotating wave shows, for nonadiabatic conditions, much higher resistance to extinction than the planar pulsating wave. For identical conditions as in Fig. 5 the pulsating front extinguishes [12]. Margolis et al. [16] indicated by using nonlinear stability analysis, that for a planar pulsating combustion front the propagation speed is lower than for a constant pattern profile regime. However, the corrugation of the reaction front can overcome the slowing effects of pulsating combustion if the space wave number is sufficiently large. This conclusion was verified by our numerical simulations.

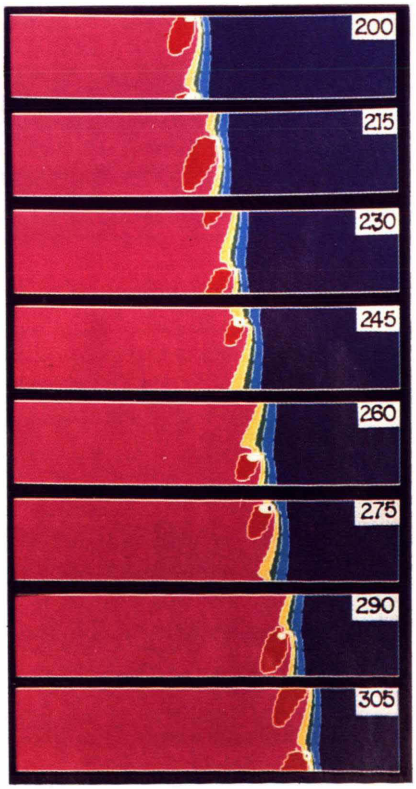

Fig. 5. One-head rotating wave (2D case), ($\beta = 0.03$, $\gamma = 0.08$, $\Theta_0 = -9.5$, $\Theta_i = 3.0$, $\nu = 0.001$, $\alpha = 0.001$).

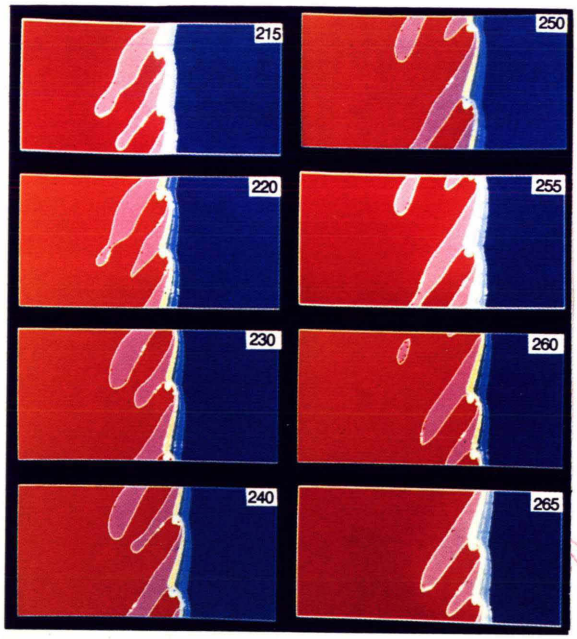

Fig. 6. Two-head rotating wave (2D case), ($\beta = 0.03$, $\gamma = 0.08$, $\Theta_0 = -9.5$, $\Theta_i = 3.0$, $\nu = 0.001$, $\alpha = 0.001$).

It was also found that for larger specimen diameter ($\nu < 5 \cdot 10^{-4}$) multihead rotating waves may be generated as predicted [7]. A two head rotating wave is shown in Figure 6. This front was formed by imposing a similar asymmetric perturbation as for the previous case of a one-head rotating wave.

Three Dimensional Simulations

The propagation of the combustion front in cylindrical pellets formed from the solid reacting components is, inherently, three dimensional. Equations (1–4) were solved in order to observe the three dimensional features of condensed systems. The set of parameters used here was identical to the one used in 2D simulations, however the results are presented in dimensional form. The diameter of the specimen was sufficiently large, so that a two head rotating wave was observed on the lateral surface similar to that shown in Figure 6. The reaction was initiated by a short time high energy pulse (laser beam) imposed on a small area of the sample. The combustion front was formed and propagated toward unreacted material. Close to the specimen center only a slightly corrugated pulsating front was observed. A one head rotating wave appeared at certain radial positions ($0.1 < \xi < 0.3$) (see Figure 7). Two head rotating wave was observed close to the lateral surface of the cylindrical sample ($0.8 < \xi < 1.0$) (see Figure 8). In the transition region between one- and two-head rotating waves the two hot spots move towards each other, collapse into one, and again reappear and move away from each other (see Figure 9). The phenomenon is periodically repeated.

Experimental Observations

Experiments were carried out to study the influence of compaction density, powder particle size, specimen dimensions and dilution on the combustion characteristics of various systems. The experimental procedure and the apparatus used is described elsewhere [17]. Several interesting nonlinear dynamic phenomena that compare well with numerical simulations were observed.

Planar Combustion Fronts

In many binary reacting systems such as molybdenum-silicon, titanium-aluminum, tantalum-boron and titanium-carbon a planar combustion front can be observed depending upon reaction conditions. In Fig. 10 a, the propagation of the reaction front for the molybdenum-silicon system is shown. It was found that the front remained stable, within the propagation limits, to variations in the specimen diameter, initial density and dilution. The axial velocity and the maximum combustion temperature were measured to be 0.004 ms^{-1} and 1850 K, respectively.

The planar characteristic of the front for the tantalum-boron systems is shown in Figure 10 b. The planar propagation in this system, in contrast to the previous one, was possible only for undiluted reaction mixtures. The reaction front velocity and the maximum combustion temperature were 0.0035 ms^{-1} and 2740 K, respectively.

The combustion processes in condensed phase systems due to their exothermicity, frequently cause very high temperatures in the reaction zone, which may lead to sintering and melting of the product. One obvious approach to reduce these high temperatures is to use inert diluents (e.g., final product). However, the process is quite sensitive to these additives and in many systems may change the combustion mode.

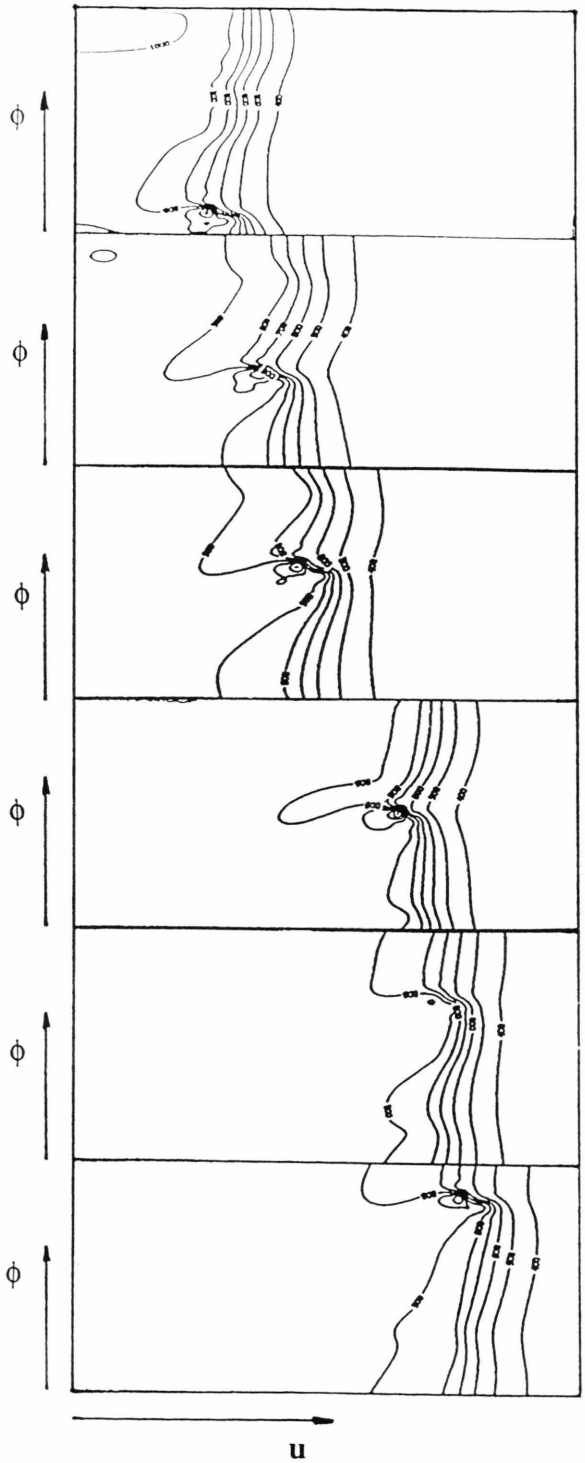

Fig. 7. One-head rotating wave (3D case), ($\beta = 0.03$, $\gamma = 0.08$, $\Theta_0 = -9.5$, $\Theta_i = 3.0$, $\nu = 0.001$, $\alpha = 0.001$). Isotherms in the (u, ϕ) plane corresponding to $\xi = 0.1$. Isotherms shown correspond to constant intervals of $\Delta T = 100$ deg ($T_{min} = 400$ deg C, $T_{max} = 1300$ deg C).

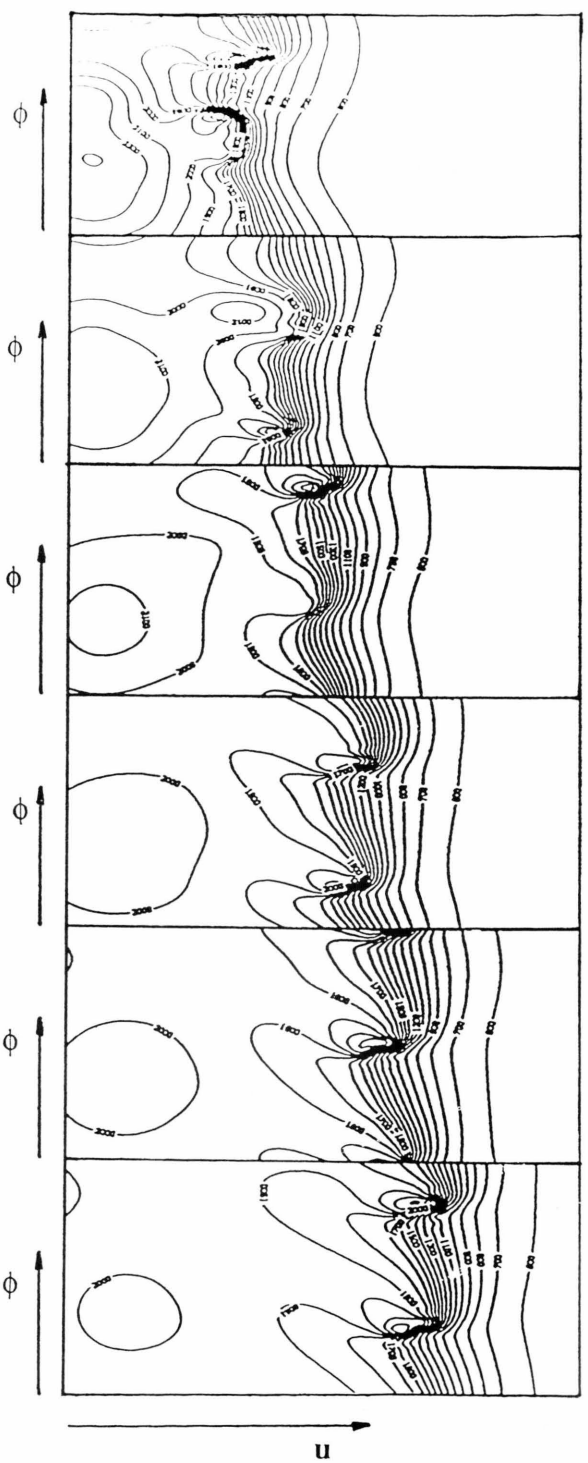

Fig. 8. Two-head rotating wave (3D case), ($\beta = 0.03$, $\gamma = 0.08$, $\Theta_0 = -9.5$, $\Theta_i = 3.0$, $\nu = 0.001$, $\alpha = 0.001$). Isotherms in the (u, ϕ) plane corresponding to $\xi = 1.0$. Isotherms shown correspond to constant intervals of $\Delta T = 100$ deg ($T_{min} = 600$ deg C, $T_{max} = 2000$ deg C).

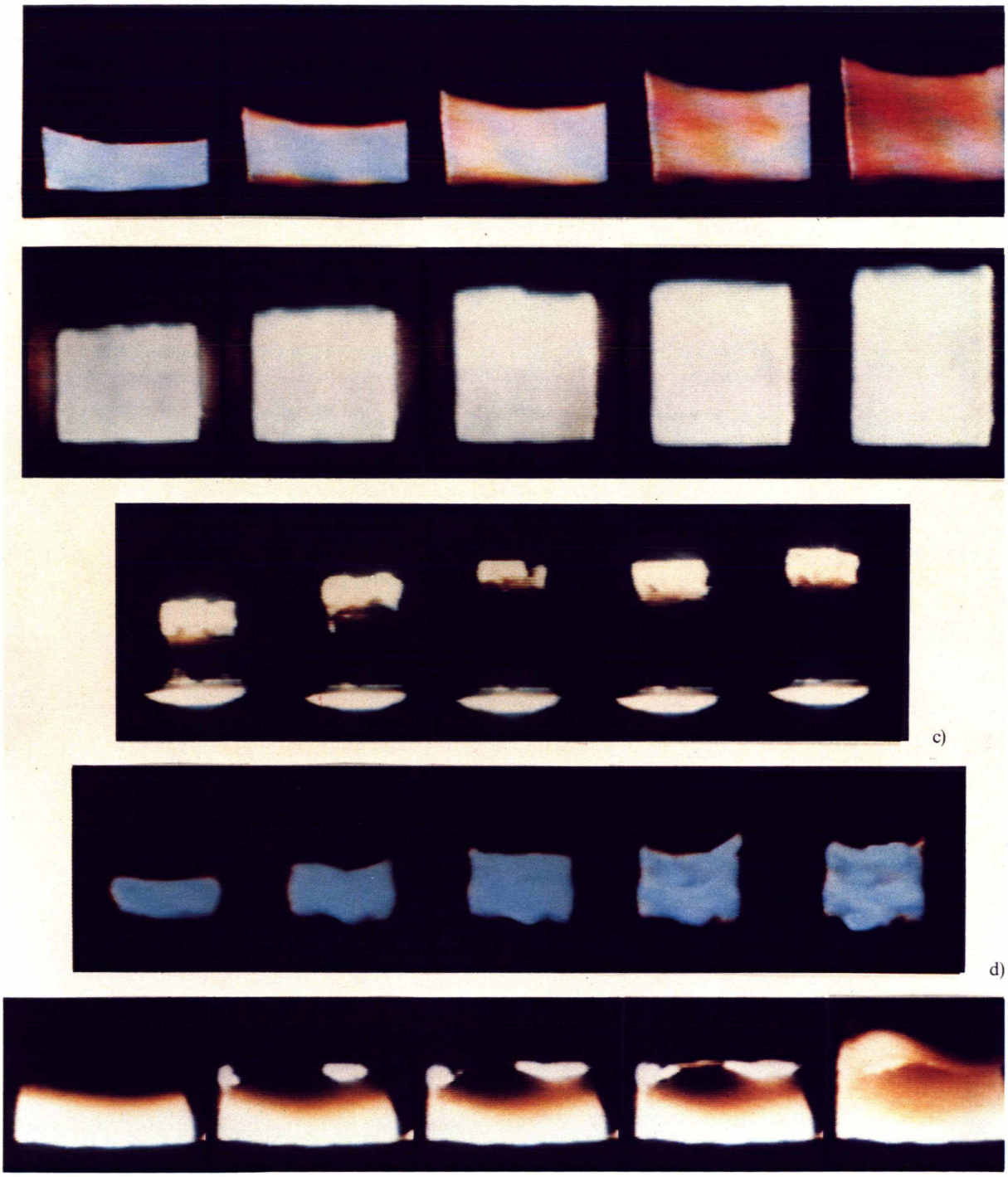

Fig. 10. Wave propagation in solid-solid systems: a) Mo–Si; b) Ta–B; c) Ta–B (25% dilution); d) Ti–B (40% dilution); e) Ti–Al. Shown are successive ride views of reacting pellets.

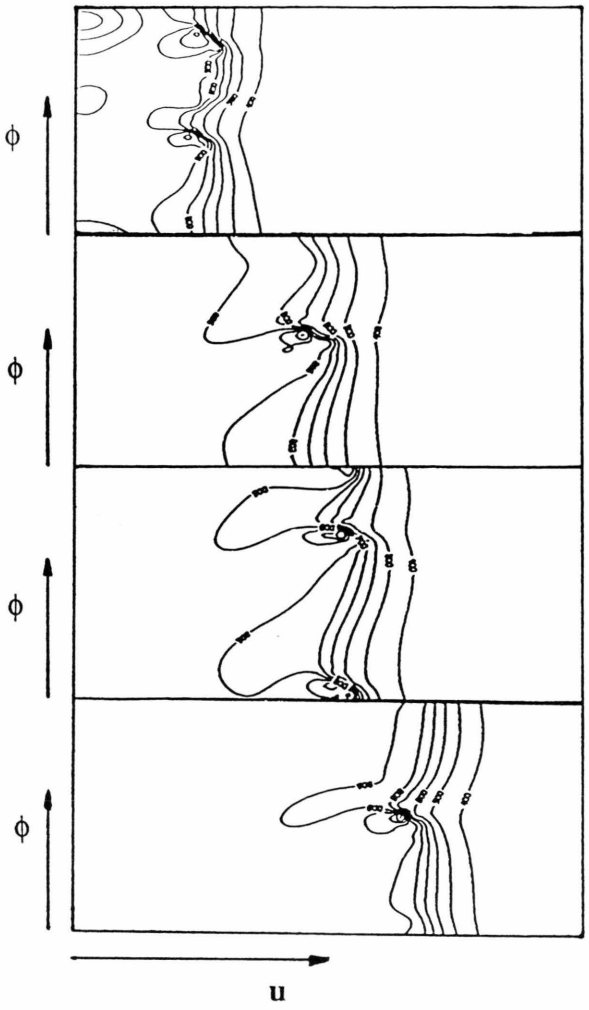

Fig. 9. Transition regime between one and two-head rotating wave (3D case), ($\beta = 0.03$, $\gamma = 0.08$, $\Theta_0 = -9.5$, $\Theta_i = 3.0$, $\nu = 0.001$, $\alpha = 0.001$). Isotherms in (u, ϕ) plane corresponding to $\xi = 0.5$. Isotherms shown correspond to constant intervals of $\Delta T = 100$ deg. ($T_{min} = 400$ deg C, $T_{max} = 1300$ deg C).

It was observed that even for the molybdenum-silicon system, high degrees of dilution led to corrugation of the reaction front, however, the average axial velocity remained constant. In other systems, strong oscillations as well as breaking of symmetry were observed.

In Fig. 10 c, a planar pulsating behavior observed for the tantalum-boron system diluted with the final product is shown. These oscillations did not seem to have affected the final conversion as revealed by X-ray diffraction phase analysis and as predicted by numerical calculations [18]. Similar phenomena were also observed for diluted titanium-carbon and titanium-aluminum systems.

Nonplanar Combustion Fronts

Higher degree of dilution and larger specimen diameter resulted in breaking of symmetry with the formation of a corrugated front for the tantalum-boron system. In Fig. 10 d such a transition from a planar to a nonplanar combustion mode is shown. No rotating wave was observed for the values of parameters investigated. However, one- and multi-head rotating waves were observed in the titanium-aluminum intermetallic system. A two-head rotating wave is shown in the Fig. 10 e, which seems to be in very good agreement with numerical predictions.

Conclusions

Solid-solid noncatalytic reactions featuring high values of both activation energy and heat of reaction, once initiated, can be self-sustaining depending on values of these parameters and operating conditions. Numerical simulations in two and three spatial dimensions reveal that different combustion modes might occur: planar constant pattern, pulsating and rotating front.

Two dimensional numerical calculations, based on a simple kinetic model, show that for non-adiabatic conditions, a rotating wave is more resistant to extiction than a planar pulsating wave. There seems to be a qualitative agreement with the experiments. However, to achieve a quantitative agreement, more precise kinetic expressions of solid-solid reactions that are accompanied by melting and other phase transformations as well as the temperature dependence of all physical parameters should be incorporated in the model equations. Three dimensional calculations, for cylindrical geometry, predict the simultaneous existence of corrugated as well as fully developed one- and two-head rotating waves depending on the radial coordinate.

Acknowledgements

This work has been supported by the NSF grands CPE 83-10627, CPE 86-10850, and by the Petroleum Research Fund 16455-AC5, that support is gratefully acknowledged.

[1] A. G. Merzhanov and I. P. Borovinskaya, Combustion Science and Technology **10,** 195 (1975).
[2] K. V. Logan and J. D. Walton, Ceramic Eng. Sci. Proceed. **5,** 712 (1984).
[3] E. I. Maksimov, A. G. Merzhanov, and V. M. Shkiro, Combustion Explosion and Shock Waves **1,** 15 (1965).
[4] I. P. Borovinskaya, A. G. Merzhanov, N. P. Novikov, and A. K. Filonenko, Combustion, Explosion and Shock Waves **10,** 2 (1974).
[5] G. I. Barenblatt, Ya. B. Zeldovich, and A. G. Istratov, Prikl. Math. Tech. Phys. **4,** 21 (1962).
[6] G. M. Makhviladze and B. V. Novozhilov, Prikl. Math. Tech. Phys. **5,** 51 (1971).
[7] G. I. Sivashinsky, SIAM J. Appl. Math. **40,** 432 (1981).
[8] B. J. Matkowsky and D. O. Olagunju, SIAM J. Appl. Math, **42,** 486 (1982).
[9] B. J. Matkowsky and G. I. Sivashinsky, SIAM J. Appl. Math. **35,** 465 (1978).
[10] S. B. Margolis, SIAM J. Appl. Math. **43,** 351 (1983).
[11] J. D. Buckmaster and G. S. S. Ludford, Lectures on Mathematical Combustion, SIAM, Philadelphia 1983.
[12] J. Puszynski, J. Degreve, and V. Hlavacek, Ind. Eng. Chem. Res. Dev. **26,** 1424 (1987).
[13] T. P. Ivleva, A. G. Merzhanov, and K. G. Shkadinskii, Fiz. Gorenija L. Vzryva **16,** 3 (1979).
[14] J. Degreve, P. Dimitriou, J. Puszynski and V. Hlavacek, Chem. Eng. Comm. **58,** 105 (1987).
[15] J. Degreve, P. Dimitriou, J. Puszynski, V. Hlavacek, S. Valone, and R. Behrens, Comp. Chem. Eng. **11,** 749 (1987).
[16] S. B. Margolis, H. G. Kaper, G. K. Leaf, and B. J. Matkowsky, Combustion Science and Technology **43,** 127 (1985).
[17] V. Hlavacek, J. Puszynski, J. Degreve, and S. Kumar, Chem. Eng. Science **41,** 877 (1986).
[18] S. Kumar, Ph.D. Thesis, SONY at Buffalo 1988.